Applied Physics A (2019) 125:341
https://doi.org/10.1007/s00339-019-2636-3

Applied Physics A
Materials Science & Processing

Near-infrared optical sensor based on band-to-band tunnel FET

Vandana Devi Wangkheirakpam[1] · Brinda Bhowmick[1] · Puspa Devi Pukhrambam[1]

Received: 4 March 2019 / Accepted: 13 April 2019 / Published online: 20 April 2019

Abstract
In this work, three different device structures based on the band-to-band tunnel field effect transistor (TFET) have been proposed for near-infrared optical sensing application. Comparison has been made on their spectral response to different wavelengths (0.7–1 μm). The device with Ge n+ pocket at the source-channel junction outperforms the other two with a better ON current I_{ON} (63.4 μA) and steeper subthreshold swing SS (28 mV/dec). Further optimization of this device is done showing influence of source doping and high-k dielectric material on its transfer characteristics. It is found that the threshold voltage V_T and I_{ON} are sensitive to wavelength variations. V_T increases by ~ 10–20 mV and I_{ON} decreases by 35% in the considered wavelength range at a gate doping of $1 \times 10^{18}/cm^3$. The sensitivity of these proposed devices are determined relative to the change in current corresponding to the change in illumination wavelength. With the utilization of Ge n+ pocket, high-k gate dielectric the peak spectral sensitivity increases to 10.53 at the illumination intensity of 0.5 W/cm^2 and also it can determine firmly separated spectral lines (100 nm) in the near infrared range because of its steep sub-threshold swing.

1 Introduction

The applications of near infrared sensors are innumerable in the fields of defense, life sciences as well as homeland security. In defense, they are mostly used for surveillance target detection, target tracking and discrimination. These functions are performed from satellites, aircraft platforms, fixed locations or inceptors [1]. Molecular detection utilizing near infrared light between 0.7 and 1.4 μm has imperative biomedical applications in view of more noteworthy tissue penetration and reduced auto-fluorescent background in the thick tissue or entire blood-media [2]. To make such kind of detection, the photo detectors should be able to differentiate closely spaced wavelengths (~ 100 nm) even if the intensity of illuminated light is less (e.g., < 1 W/cm^2). Both theoretical and experimental studies have been performed on metal oxide semiconductor field effect transistors (MOSFETs) for different types of optically control applications [3]. The MOSFETs based photo detectors are found to be more beneficial in comparison with avalanche photo diodes. The carriers generated in the gate due to incident light modulate the current in the device [4]. Detection of firmly separated spectral lines at lesser illumination intensity of the incident light requires the FET sensors to show current variation with the variation in the effect of gate caused by varying the wavelength of incident light. This is determined by the subthreshold swing (SS) and hence it controls the sensitivity of the FET-based sensors [2]. Unlike avalanche photodiodes, which require greater electric fields (20 V/μm) to acquire desired rate of ionization, the MOSFETs based detectors have separate absorbing and conducting regions. These type of sensors also have high compatibility for integrated circuit, low power operation and higher noise performance leading to an increase in their sensing capabilities to a greater extend [5], [6]. However, the minimum achievable sub-threshold swing for conventional MOSFETs is limited to 60 mV/dec at room temperature. In this regard, tunnel field effect transistor (TFET) has become a device of interest as it possesses the potential to replace MOSFETs [7]. The band-to-band tunnelling (BTBT) mechanism on which the TFET operates allows it to exhibit low sub-threshold swing and low leakage current [8–10]. Such characteristics of the TFET makes it a promising emerging device not only for low power applications but also for bio-sensing and light sensing applications [11–14].

This work presents a three different structural designs and simulation of optoelectronic band-to-band tunnel field effect transistor (TFET) for near-infrared

✉ Vandana Devi Wangkheirakpam
vannawang46@gmail.com

[1] Department of Electronics and Communication Engineering, National Institute of Technology, Silchar, Silchar, Assam 788010, India

light sensing application in the wavelength (λ) range of 700 nm–1 µm. This work also reports the behaviour of the device structure under illumination and dark condition. The device performance is analysed using Synopsys Sentaurus Device TCAD tool [15]. Although TFETs have good SS, concerns are still there regarding its low ON current [16]. To improve the ON current of the device and make it a reliable device for commercial usage, a slight modification is made in the geometry of the device [17–19]. The source is replaced with a Germanium source and a Germanium pocket is included on the source side of the proposed device structure allowing a vertical tunnelling normal to the gate-oxide thickness, in addition to the lateral one [20]. In addition, comparison has been made on the spectral response of these devices. Moreover, the influence of different device parameters such as doping, high-k dielectric on the device characteristic has been studied in this work. Furthermore, the performance of the device is analysed in terms of spectral sensing capacity using TCAD simulation.

2 Device structure and principle of operation

Figure 1a–c show the schematics of the proposed devices. All the three devices have highly a doped n-type silicon gate along with band-to-band TFET structure. The photons get absorbed in these photon sensing regions of the gate and optical generation takes place in this region. The illumination windows in the proposed device structures are defined in the region,

$$\{-(W_g + t_{ox}) \le x \le (-t_{ox})\}.$$

The device considered in Fig. 1a is a silicon n-type TFET. It comprises of a silicon n-type photon absorbing gate, p-type Si source, intrinsic Si channel and an n-type Si drain. The proposed device is basically a band-to-band tunnel FET where carrier transitions are taking place from the valence band of the p-type Si source (p-Si) to the conduction band of the intrinsic Si channel (i-Si). Table 1 summarizes the structural parameters used in this work.

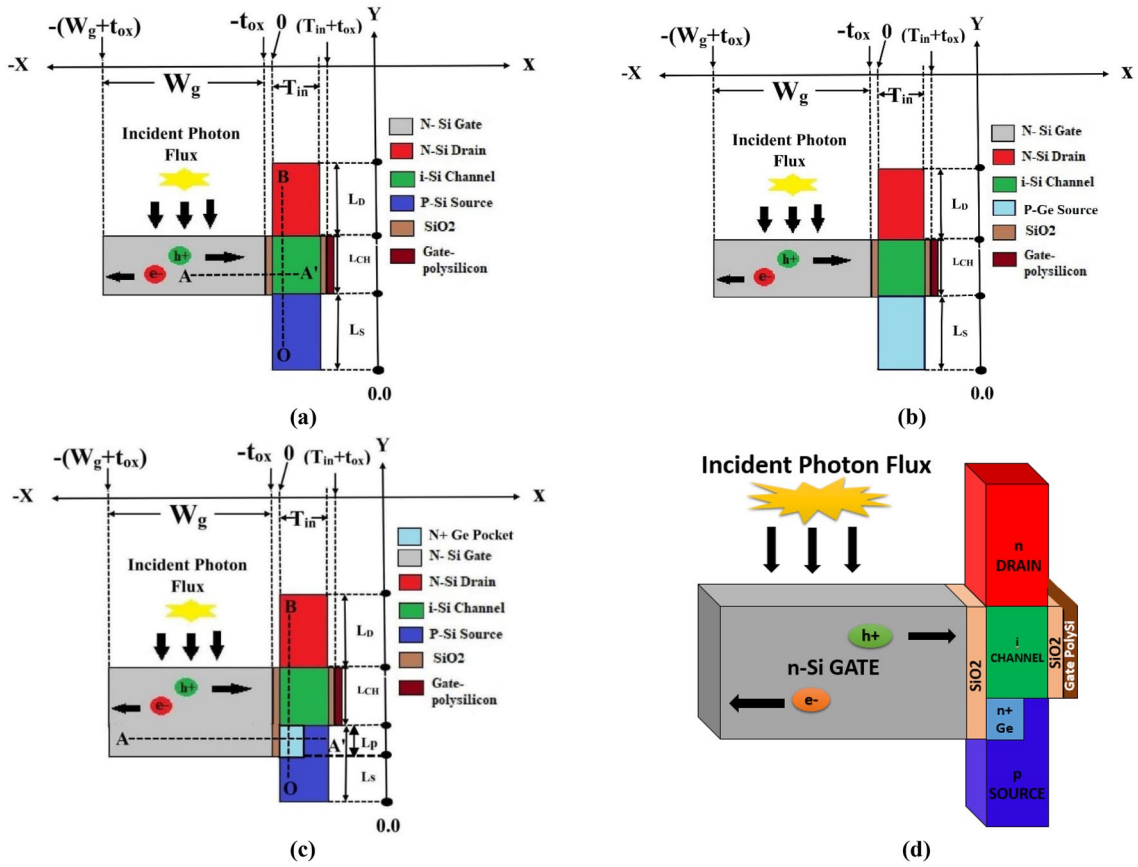

Fig. 1 Schematic of the proposed TFET device structures **a** Si source (conventional), **b** with Germanium p-type source, **c** Si source with Germanium pocket at the source side allowing both vertical and lateral tunnelling. **d** A 3D illustration for the device proposed in **c**

Table 1 Device structural parameters used in simulation

Parameters	Value
Length of illumination window of the gate (W_g)	50 nm
Length of channel (L_{CH})	30 nm
Length of drain (L_D)	35 nm
Length of source (L_S)	35 nm
Gate-oxide thickness (t_{ox})	2 nm
Thickness of the silicon substrate (T_{in})	10 nm
Thickness of the gate region (Fig. 1a, b)	30 nm
Thickness of the gate region (Fig. 1c)	45 nm
Pocket length (L_p for Fig. 1c)	15 nm
Pocket thickness (Fig. 1c)	3 nm
Donor doping concentration in N-Si gate	$4 \times 10^{19}/cm^3$
Donor doping concentration in N-Ge pocket	$1 \times 10^{19}/cm^3$
Donor doping concentration in N-Si drain	$1 \times 10^{18}/cm^3$
Channel doping concentration	$1 \times 10^{15}/cm^3$
Donor doping concentration of N-Si gate (Ng)	$1 \times 10^{19}/cm^3$

At the illuminated condition, when incident light arrives normal to the illumination window, generation of excess electron–hole pairs (EHPs) takes place in the gate region. Photons having energy higher than the forbidden bandgap energy of Si will get absorbed and as a result photo-generation took place. The applied gate bias (V_{GS}) along with the band bending in the gate region is reason behind the process of the photo-generated carriers flow inside the gate region. When a positive gate voltage V_{GS} is applied to the device, photo-generated electrons inside the gate will attract towards the electrode, whereas the excess holes get accumulated near the gate/gate-oxide interface. This process disturbs the equilibrium in the gate region resulting in the separation of quasi-Fermi energy levels of electron (Efn) and hole (Efp) giving rise to a net photo-voltage (V_{OP}) across it. Figure 2a shows this separation of quasi-Fermi energy levels taken along the cutline AA′ inside the gate region, in the ON state ($V_{GS}=1.5$ V and $V_{DS}=1$ V) energy band diagram, at the illumination intensity of 0.5 W/cm^2 ($\lambda=0.7$ µm). However, Efn and Efp overlap with each other under the dark condition, as shown in Fig. 2b. This proves that the under dark condition the equilibrium is not disturbed.

In addition to the applied gate bias V_{GS}, the photo-voltage also contributes as another gate bias lowering the turn ON voltage (V_{ONSET}) required for band-to-band tunneling to take place between the source and the channel region. Consequently, at the illumination condition the tunneling current increases. Another gate at the back of the device is used to increase the gate control over the device. A good ON current is required to increase the speed of the device which in turn increases the device sensitivity. Further increment in the ON current is found by introducing a Germanium p-type source and the modified structure is

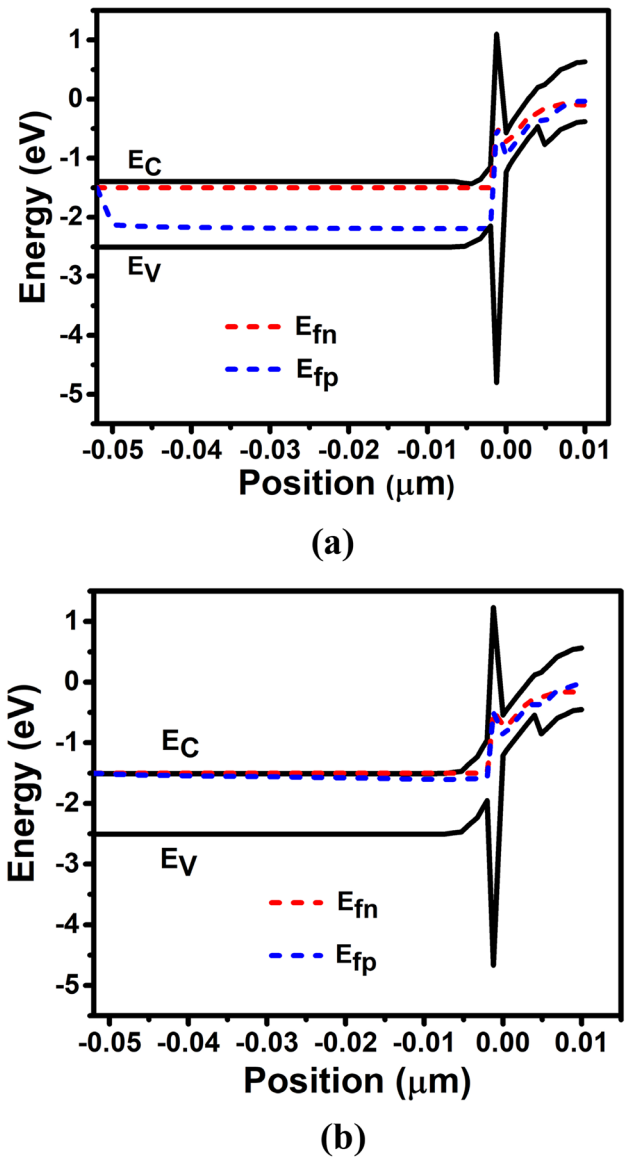

Fig. 2 **a** Energy band diagram taken along the cutline AA′ for ON state ($V_{GS}=1.5$ V and $V_{DS}=1$ V) obtained at illumination intensity $I=0.5$ W/cm^2 and $\lambda=0.7$ µm (Fig. 1c), showing the Efn and Efp in the gate region. **b** Band diagram along cutline AA′ observed at the dark condition

shown in Fig. 1b. Use of lower band gap materials such as Ge in the source side offers higher BTBT leading to an improvement in the ON state current (I_{ON}). We also proposed an improved structure where, an $n+$Ge pocket is included creating a hetero-junction at the source–channel junction of the device as shown in Fig. 1c. Since Ge has a lower band gap, tunneling increases at the source-pocket junction parallel to the gate-oxide. This tunnelling is referred to as the lateral tunnelling. Besides this lateral tunnelling, an additional tunnelling is observed perpendicular to the gate-oxide referred to as the vertical

tunnelling. Complex refractive index model is used for the optical generation on the device. The optical generation and intensity plots are depicted in Fig. 3a, b. Schenk model is used to account for intrinsic carrier concentration required in SRH (Shockley–Read–Hall) expressions. The effects of high doping are simulated using band gap narrowing model. The characteristics of these devices are studied from 2-D numerical simulations results which are obtained by using TCAD simulator Sentaurus-device tool. However, for better understanding of the device structure, a 3D illustration of the proposed device with $n+$Ge pocket (Fig. 1c) is given in Fig. 1d.

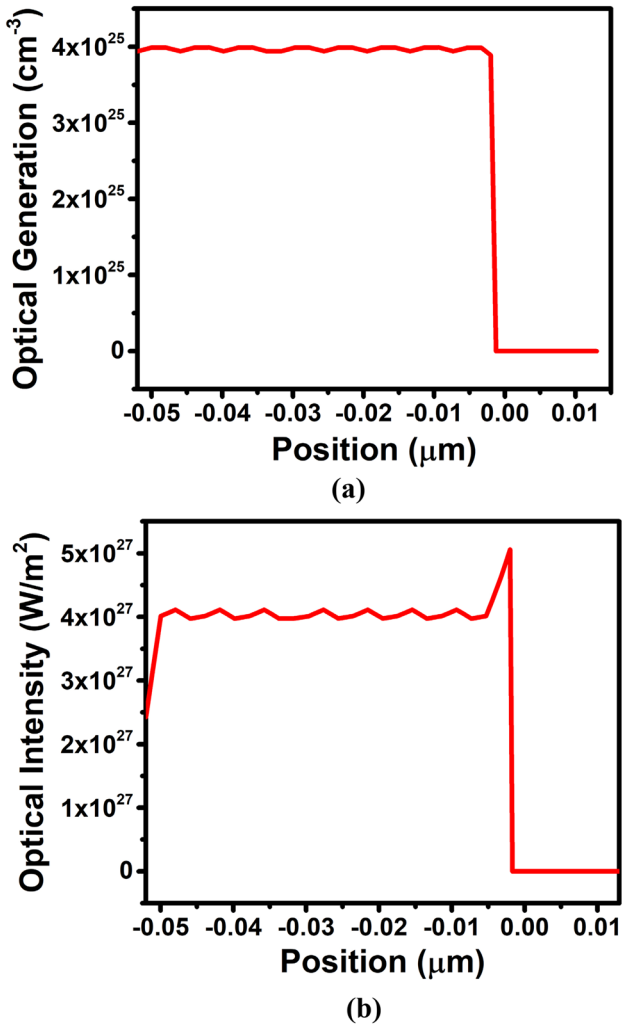

Fig. 3 **a** Optical generation occurring at the gate region due to the illuminated light ($I=0.5$ W/cm^2 and $\lambda=0.7$ μm), **b** corresponding optical intensity

3 Results and discussion

The BTBT parameters for Si are provided in the simulation tool. Experimentally calibrated optical parameters for Ge, reported in Ref. [22], are used to simulate the device structures in Fig. 1b, c. The sub-threshold swing of the device is calculated using the formula

$$\mathrm{SS} = \left(\frac{\mathrm{d}\log I_{\mathrm{D}}}{\mathrm{d}V_{\mathrm{GS}}}\right)^{-1}. \tag{1}$$

The spectral sensitivity (Sn) of the device depends on the drain current I_{DS} and it can defined as the ratio of difference in drain current I_{DS}, when illumination wavelength reduces from λ_2 to λ_1, to the drain current of the initial wavelength I_{DS}. This is given by Eq. (2) below.

$$\mathrm{Sn} = \frac{I_{\mathrm{DS}}(\lambda_1)}{I_{\mathrm{DS}}(\lambda_2)} - 1. \tag{2}$$

The work does not consider the non-ideal effects such as defect assisted tunneling.

3.1 Spectral response of the device

Figure 4 shows the spectral response of the three device structures. Comparison has been made based on their I_{D}–V_{GS} characteristics. These characteristics are obtained under illumination condition i.e. $I=0.5$ W/cm^2 for different values of wavelength λ where V_{DS} is fixed at 1 V and V_{GS} is varying from 0 to 2 V. These simulated plots exhibit similar trend of reduction in I_{ON} and a slight increment in V_{ONSET}. In case

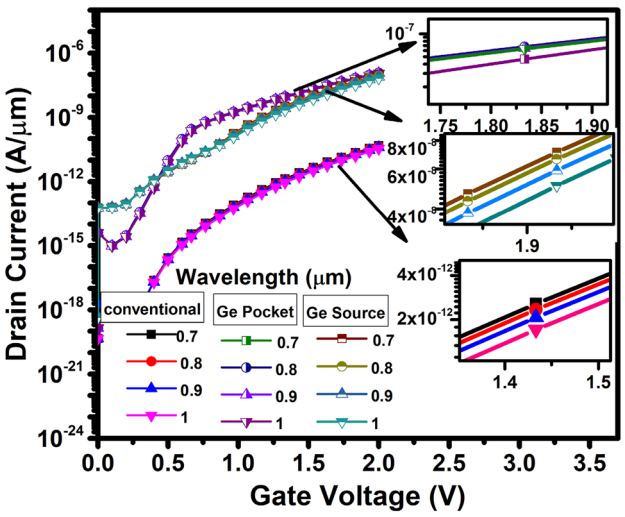

Fig. 4 Spectral response of the three proposed devices obtained at $I=0.5$ W/cm^2 for different values of wavelength at $V_{\mathrm{DS}}=1$ V and $V_{\mathrm{GS}}=2$ V

of the conventional device, the I_{ON} extracted from these transfer characteristics curves increases from 3.41×10^{-11} to 5.74×10^{-11} A when wavelength λ decreases from 1 to 0.7 µm. This is because as λ decreases, the photo-generation in the gate region increases [21]. Consequently, the optical voltage V_{OP} increases, which in turn reduces the V_{ONSET}. Using Ge p-type source the response shows the increase of ON current from 6.7×10^{-8} to 9.4×10^{-8} A and finally the third device proposed with Ge n+ pocket gives an increment from 1.12×10^{-8} to 6.4×10^{-8} A in the considered wavelength range.

Figure 5 shows the comparative plots of the simulated transfer characteristics of the three different structure given in Fig. 1a–c at $V_{GS} = 1.5$ V, $V_{DS} = 1$ V and $\lambda = 0.7$ µm. The conventional device structure with Si source shows comparatively lower ON current I_{ON} due to its large band gap nature, by introducing Ge p-type source which has a lower bandgap, the on state current of the device can be improved which is shown in Fig. 5. This structural modification increases the current from 8.74×10^{-12} to 9.2×10^{-9} A/µm. Doping concentration of $1 \times 10^{19}/cm^3$ Germanium p-type source is included with i-Si channel, n-Si drain and n-Si gate (Fig. 1b). However, the subthreshold swing increases from 47 (conventional) to 62 mV/dec. The third curve shows the transfer characteristics of the device which has a Si source with Ge pocket (Fig. 1c). This structure gives comparatively good result with improved current as well as the SS. In this structure, the inclusion of n + Ge pocket at the source-channel junction provides an extra tunnelling path normal to the gate-oxide thickness. The channel, drain and gate remain same for all the proposed device structures. Hence, both lateral and vertical tunnelling in this device enables more electrons to reach the drain side. This provides an improvement in the on state current and SS (I_{ON} of 58 nA/µm and SS of 36 mV/dec).

Figure 6 depicts the Sn–V_{GS} characteristics plots corresponding to λ values (1 µm and 0.7 µm). Spectral sensitivity in this plot is calculated using Eq. (2) utilizing the appropriate pair of simulated transfer characteristic curves. It can be seen from the figure that for conventional structure Sn reaches the peak value 0.511 at $V_{GS} = 1.1$ V and starts decreasing with V_{GS} beyond that.

This is due to the gradual saturation of the I_D–V_{GS} curve leading to the increase in SS. For the case of Ge p-type source, the peak response of 0.567 is obtained at $V_{GS} = 1.3$ V. The gate voltage required to reach the peak spectral response increases due to its higher SS. The device using Ge n+ pocket reaches its peak value of 0.45 at $V_{GS} = 0.9$ V. Because of its steeper SS and lower threshold voltage V_T in comparison with the other two, the change in drain current with the change in wavelength (Eq. 2) for this device is more at the lower gate voltage. So, it reaches the peak sensitivity at lesser $V_{GS.}$ Moreover, due to its high ON current and better I_{ON}/I_{OFF}, the speed of this Silicon source Germanium pocket device will be more than the other two. Hence, the latter device outperforms the other two in terms of ON current and SS.

However, the sensitivity obtained is less. This is not only because of the insignificant increase in V_T with wavelength but also the low ON current I_{ON} (58 nA/µm) obtained for this device which is a disadvantage of conventional tunnel FET. To improve this I_{ON} and the device sensitivity, optimization of the device structures using inclusion of hetero-junction, use of lower band-gap materials, high-*k* dielectric materials,

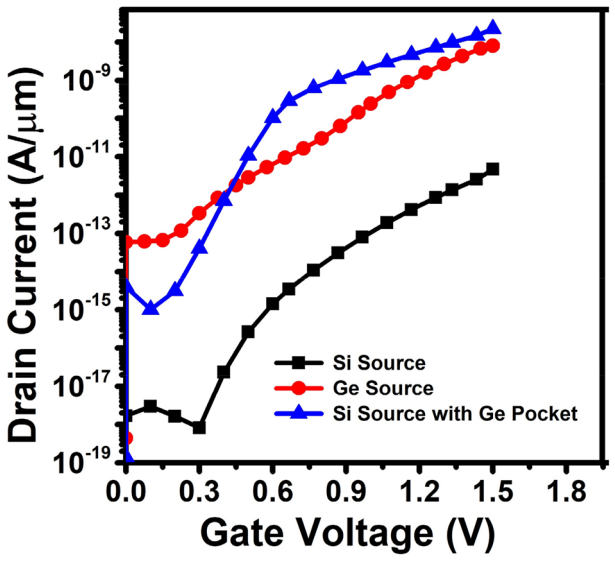

Fig. 5 The transfer characteristics comparison for the three different structures at $\lambda = 0.7$ µm

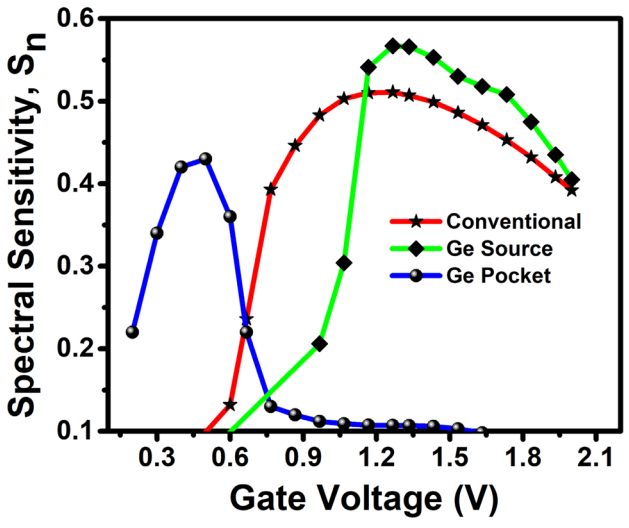

Fig. 6 Variation of spectral sensitivity, Sn with applied gate voltage V_{GS} at illuminated condition when $V_{GS} = 2$ V, $V_{DS} = 1$ V and λ changes from 1 to 0.7 µm

vertical TFET, etc. can be done. These are illustrated in the following sections.

3.2 Optimization of the Ge n+ pocket TFET sensor

The proposed Ge pocket structure is optimized by considering the influence of source doping and high-*k* gate dielectric.

3.2.1 Influence of source doping

Increasing source doping concentration of the device can increase ON current I_{ON} to a greater extend with lesser subthreshold swing. Figure 7 demonstrates the TCAD simulation results of I_D–V_{GS} characteristics of the device with various doping concentrations of source, fixing channel, pocket and drain doping concentrations at 1×10^{15}/cm^3, 1×10^{19}/cm^3 and 1×10^{18}/cm^3, respectively, at $V_{GS}=2$ V, $V_{DS}=1$ V and $\lambda=0.7$ µm. The ON current I_{ON} shoots up-to 54 µA/µm when source doping is 2×10^{19}/cm^3.

The electric field at source and channel junction increases with the increase in source doping. Because of this, there is an improvement in the ON current I_{ON} which can be seen from the transfer characteristics. Tunneling barrier width also reduces with higher source doping resulting in an enhancement of I_{ON}.

3.2.2 Effect of high-*k* dielectric

Furthermore, the oxide material SiO_2 of the device is replaced with high-*k* dielectric material HfO_2 with the dielectric constant of 22. Careful choice of dielectric materials can also improve the ON current of the device. I_{ON} can also be improved by scaling the oxide thickness. However, scaling down the thickness of the gate dielectric SiO_2 beyond 1–1.5 nm leads to the enhancement of gate leakage current. Using high-*k* dielectric materials, the gate control on the device can be improved. In Fig. 8, it is observed that a better current and a steeper SS (28 mV/dec) are achieved by utilizing HfO_2. Here, the oxide thickness tox of 2 nm is taken in both the case.

3.2.3 Spectral response of the device

Figure 9 shows the plots of spectral response of the device in terms of its I_{DS}–V_{GS} characteristics with an SS of 28 mV/dec. The transfer characteristics are obtained at $V_{DS}=1$ V for Ng $=4\times10^{19}$/cm^3 and V_{GS} is varying from 0 to 1.5 V. The spectral response is observed at the illuminated condition where the wavelength is varying from 0.7 to 1 µm. The nature of the plots shows slow saturation of drain current. This is because of the variation in electron quasi-Fermi potential caused by the potential drop at the channel region and the gradual change of its tunneling probability.

Figure 10 shows the plots of threshold voltage V_T and I_{ON} with the wavelength of incident photon which is varying from 0.7 to 1 µm. V_T is plotted from the I_D–V_{GS} characteristic curves shown in Fig. 9 at $V_{DS}=1$ V using constant current method (10^{-7} A/µm). I_{ON} is also taken out from the corresponding I_D–V_{GS} curves at $V_{GS}=1.5$ V, $V_{DS}=1$ V and $I=0.5$ W/cm^2. Increasing the illumination wavelength λ causes a reduction in the absorption coefficient (α) per unit length of the region where photon sensing took place. This reduces the optical generation

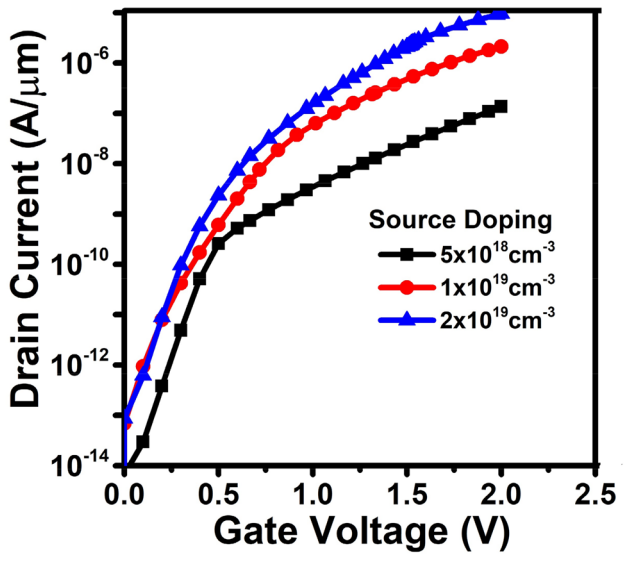

Fig. 7 Effect of acceptor source doping concentration on the device structure 3 at $V_{GS}=2$ V, $V_{DS}=1$ V and $\lambda=0.7$ µm

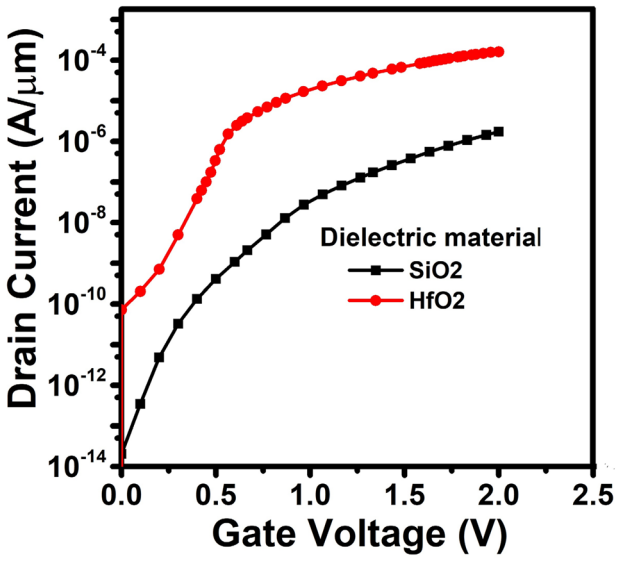

Fig. 8 Transfer characteristic plots using SiO_2 and high-*k* dielectric material ($k=22$) for structure 3 at $V_{GS}=2$ V, $V_{DS}=1$ V and $\lambda=0.7$ µm

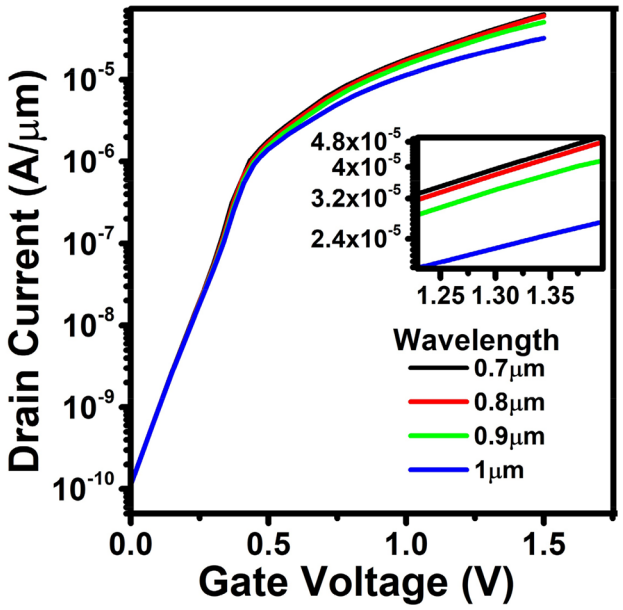

Fig. 9 Plots showing simulated transfer characteristics for the device structure with Ge n+pocket (structure 3 Fig. 1c) obtained at $I=0.5$ W/cm^2 for different values of wavelength at $V_{DS}=1$ V and $V_{GS}=1.5$ V

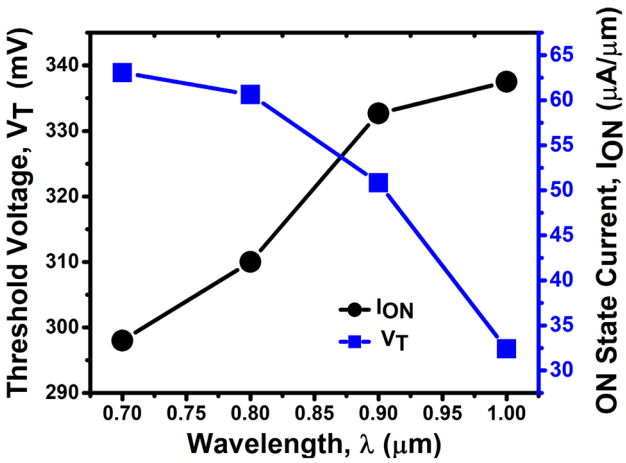

Fig. 10 Plots of variation of V_T and I_{ON} with incident photon wavelength λ. Both V_T and I_{ON} are obtained from the TCAD simulation results of I_D–V_{GS} characteristic plots at $V_{DS}=1$ V, $V_{GS}=1.5$ V and $I=0.5$ W/cm^2. Ng is chosen to be 1×10^{18}/cm^3

in that particular region of the gate when the values of λ are increased. Consequently, the optical voltage V_{op} in the gate region reduces which causes an increase of V_T and reduction in I_{ON}, as can be observed from Fig. 10. V_T increases by ~ 10–20 mV for the illumination wavelength $\lambda_1=0.7$ μm and $\lambda_2=1$ μm. Similarly, a decrement of about 35% of I_{ON} has been depicted from the graph. This reduction in the current can be seen from the band diagram

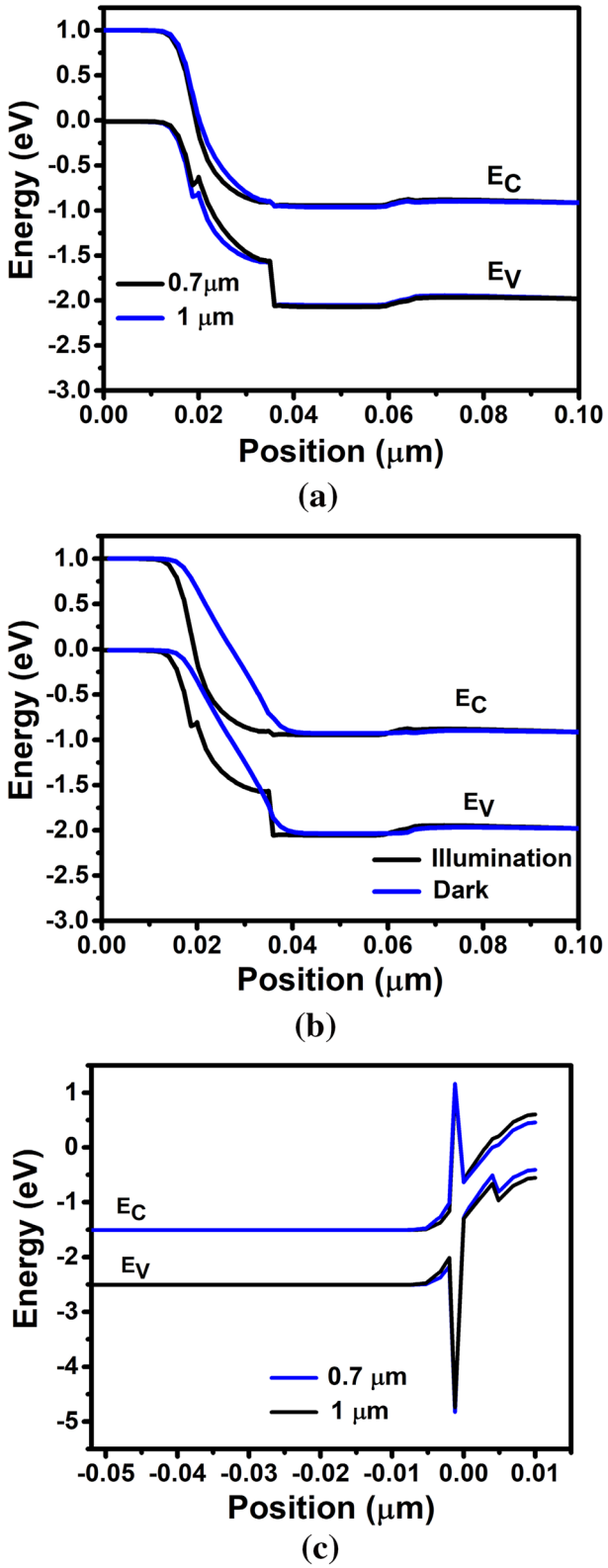

Fig. 11 **a** Energy band diagram at illumination condition obtained for $\lambda=0.7$ μm and $\lambda=1$ μm taken along OB. **b** Energy band diagram obtained for dark and illumination condition taken at lateral direction. **c** Corresponding band diagram along the vertical direction AA′ for $\lambda=0.7$ μm and $\lambda=1$ μm

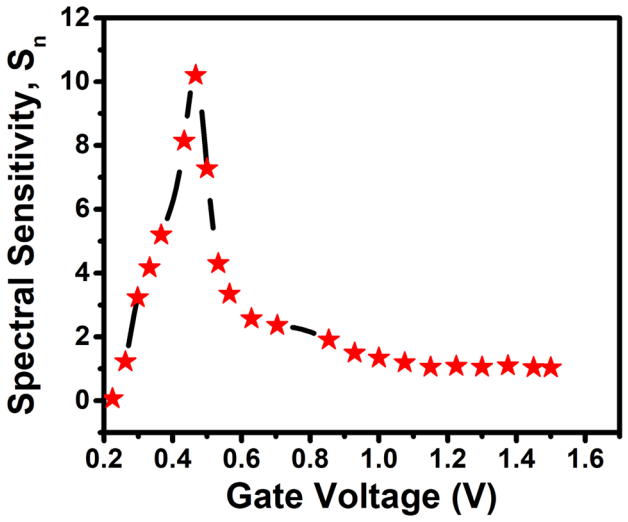

Fig. 12 Variation of spectral sensitivity, Sn with the applied gate voltage V_{GS} at the $I = 0.5$ W/cm^2 (for $\lambda_1 = 0.7$ µm and $\lambda_2 = 1$ µm)

given in Fig. 11 which shows the comparison of the BTBT tunnelling occurring at the source side at $\lambda = 0.7$ µm and $\lambda = 1$ µm. It is observed from Fig. 11a that the lateral BTBT width is more narrow for $\lambda = 0.7$ µm which causes more I_{ON} in this case. Figure 11b shows the band diagrams in the lateral direction OB for dark and illumination condition. The tunnelling width is more in the dark condition as compared to the illuminated condition, and hence, fewer electrons can tunnel from the valence band of the source to the conduction band of the channel thereby giving less current. Similarly, the difference in the vertical tunnelling across the line AA′, at wavelengths 0.7 µm and $\lambda = 1$ µm is presented in Fig. 11c. Figure 11a, c show more tunnelling for lower values of wavelengths.

Spectral sensitivity (Sn) of the device with source doping 5×10^{19}/cm^3, HfO_2 as gate dielectric, is calculated using Eq. (2) for the change of wavelength from λ_2 to λ_1.

Figure 12 shows the variation of Sn with V_{GS}, obtained from the corresponding I_{DS}–V_{GS} characteristic ($I = 0.5$ W/cm^2). The result is obtained at the illuminated condition for $\lambda_1 = 0.7$ µm and $\lambda_2 = 1$ µm, and it is observed that Sn first increases and then decreases significantly at higher values of V_{GS}. This decrease is because of the steady increase in SS when the device operates from the sub-threshold region to the super-threshold region with increase in V_{GS}. The peak spectral sensitivity is found to be 10.53 for the optimized proposed Ge pocket device, for the wavelength pairs considered in the observation.

4 Conclusion

In this work, three different structures of photosensitive TFETs are presented for near—infrared optical sensing applications. The structures are designed for band-to-band tunnelling from the valence band of the source to the conduction band of the channel causing transfer of electron from source to drain at the illuminated condition ($I = 0.5$ W/cm^2). The device structure proposed with Ge n+ pocket outperforms the other two in terms of ON current and SS. It provides comparatively higher ON current of 63.4 µA with a steeper SS of 28 mV/dec. This work also shows an improvement of peak spectral sensitivity, Snm to 10.53 by optimizing the Ge n+ pocket TFET device parameters in the wavelength range 0.7–1 µm. The spectral sensitivity decays with applied gate voltage V_{GS} due to the gradual saturation of the transfer characteristics curve. TCAD simulation results of the device shows an improved I_{ON} with the utilization of high-k dielectric material and increase in the source doping. Thus, this device can be a promising emerging device for near-infrared sensing and imaging applications.

Acknowledgements The authors acknowledge the Project CSIR EMR-II, sanction no. 22(0737)/17/EMR-II for providing necessary facilities to carry out the research work.

References

1. S. Pleasants, Exploiting the infrared. Nat. Photon. **8**, 351 (2014)
2. J.H. Correia, G. de Graaf, M. Bartek, R.F. Wolffenbuttel, A single-chip CMOS optical micro spectrometer with light-to-frequency converter and bus interface. IEEE J. Solid State Circuits **37**, 1344–1347 (2002)
3. E. Lee, D. Moon, J. Yang, K.S. Lim, Y. Choi, Transparent zinc oxide gate metal–oxide–semiconductor field-effect transistor for high-responsivity photodetector. IEEE Electron Device Lett. **30**, 493–495 (2009). https://doi.org/10.1109/LED.2009.2016765
4. H. Eltoukhy, K. Salama, A. El Gamal, A 0.18-µm CMOS bioluminescence detection lab-on-chip. IEEE J. Solid State Circuits **41**, 651–662 (2006)
5. L. Colace, G. Masini, G. Assanto, Ge-on-Si approaches to the detection of near-infrared light. IEEE J. Quantum Electron **35**, 1843–1852 (1999)
6. A.K. Okyay, D. Kuzum, S. Latif, D.A.B. Miller, K.C. Saraswat, Silicon germanium CMOS optoelectronic switching device: bringing light to latch. IEEE Trans. Electron Devices **54**, 3252–3259 (2007)
7. W.Y. Choi, B. Park, J.D. Lee, T.K. Liu, Tunneling field-effect transistors (TFETs) with subthreshold swing (SS) less than 60 mV/dec. IEEE Electron Device Lett. **28**, 743–745 (2007). https://doi.org/10.1109/LED.2007.901273
8. K.K. Bhuwalka, S. Sedlmaier, A.K. Ludsteck, C. Toksdorf, J. Schulzeand, I. Eisele, Vertical tunnel field-effect transistor. IEEE Trans. Electron Devices **51**, 279–282 (2004). https://doi.org/10.1109/ted.2003.821575
9. S. Wirths, A.T. Tiedemann, S. Trellenkamp, D. Buca, Q.T. Zhao, S. Mantl, Novel SiGe/Si line tunneling TFET with high I_{ON} at low

V_{DD} and constant SS, in Proc. IEDM 608–611 (2015). https://doi.org/10.1109/iedm.2015.7409757
10. Q. Huang, R. Huang, C. Wu, H. Zhu, C. Chen, J. Wang, L. Guo, R. Wang, L. Ye, Y. Wang, Comprehensive performance reassessment of TFETs with a novel design by gate and source engineering from device/circuit perspective, in Proc. IEDM 335–338 (2014). https://doi.org/10.1109/iedm.2014.7047044
11. G. Zhou, R. Li, T. Vasen, M. Qi, S. Chae, Y. Lu, Q. Zhang, H. Zhu, J.-M. Kuo, T. Kosel, M. Wistey, P. Fay, A. Seabaugh, H. Xing, Novel gate-recessed vertical InAs/GaSb TFETs with record high I_{ON} of 180 μA/μm at $V_{DS}=0.5$ V, in Proc. IEDM, 777–780 (2012). https://doi.org/10.1109/iedm.2012.6479154
12. R. Narang, M. Saxena, R.S. Gupta, M. Gupta, Dielectric modulated tunnel field-effect transistor—a biomolecule sensor. IEEE Electron Device Lett. **33**, 266–268 (2012)
13. D. Sarkar, K. Banerjee, Proposal for tunnel-field-effect-transistor as ultra-sensitive and label-free biosensors. Appl. Phys. Lett. **100**, 143108 (2012)
14. M. Verma, S. Tirkey, S. Yadav, D. Sharma, D.S. Yadav, Performance assessment of a novel vertical dielectrically modulated TFET-based biosensor. IEEE Trans. Electron Devices **64**, 3841–3848 (2017)
15. Sentaurus Device User Guide, *Version G-2012.06* (Synopsys, Inc., Mountain View, 2012)
16. R. Goswami, B. Bhowmick, An algorithm for extraction of threshold voltage in heterojunction TFETs. IEEE Trans. Nanotechnol. **78**, 92 (2017). https://doi.org/10.1109/tnano.2016.262877
17. W.V. Devi, B. Bhowmick, Optimisation of pocket doped junctionless TFET and its application in digital inverter. Micro Nano Lett. (2018). https://doi.org/10.1049/mnl.2018.5086
18. F. Chen, H. Ilatikhameneh, Y. Tan, G. Klimeck, R. Rahman, Switching mechanism and the scalability of vertical-TFETs. IEEE Trans. Electron Devices **65**, 3065–3068 (2018). https://doi.org/10.1109/TED.2018.2831688
19. M.A. Raushan, N. Alam, M.J. Siddiqui, Performance enhancement of junctionless tunnel field effect transistor using dual-*k* spacers. J. Nanoelectron. Optoelectron. (2018). https://doi.org/10.1166/jno.2018.2334
20. E. Memisevic, J. Svensson, E. Lind, L. Wernersson, Vertical nanowire TFETs with channel diameter down to 10 nm and point S MIN of 35 mV/decade. IEEE Electron Device Lett. **39**, 1089–1091 (2018). https://doi.org/10.1109/LED.2018.2836862
21. P.S. Gupta, S. Chattopadhyay, P. Dasgupta, H. Rahaman, A novel photosensitive tunneling transistor for near-infrared sensing applications: design, modeling, and simulation. IEEE Trans. Electron Devices **62**, 1516–1522 (2015). https://doi.org/10.1109/TED.2015.2414172
22. D.E. Aspnes, A.A. Studna, Dielectric functions and optical parameters of Si, Ge, GaP, GaAs, GaSb, InP, InAs. Phys. Rev. B **27**, 985 (1983)